JAAS

Accepted Manuscript

This is an *Accepted Manuscript*, which has been through the Royal Society of Chemistry peer review process and has been accepted for publication.

Accepted Manuscripts are published online shortly after acceptance, before technical editing, formatting and proof reading. Using this free service, authors can make their results available to the community, in citable form, before we publish the edited article. We will replace this *Accepted Manuscript* with the edited and formatted *Advance Article* as soon as it is available.

You can find more information about *Accepted Manuscripts* in the Information for Authors.

Please note that technical editing may introduce minor changes to the text and/or graphics, which may alter content. The journal's standard Terms & Conditions and the Ethical guidelines still apply. In no event shall the Royal Society of Chemistry be held responsible for any errors or omissions in this *Accepted Manuscript* or any consequences arising from the use of any information it contains.

ROYAL SOCIETY OF CHEMISTRY

www.rsc.org/jaas

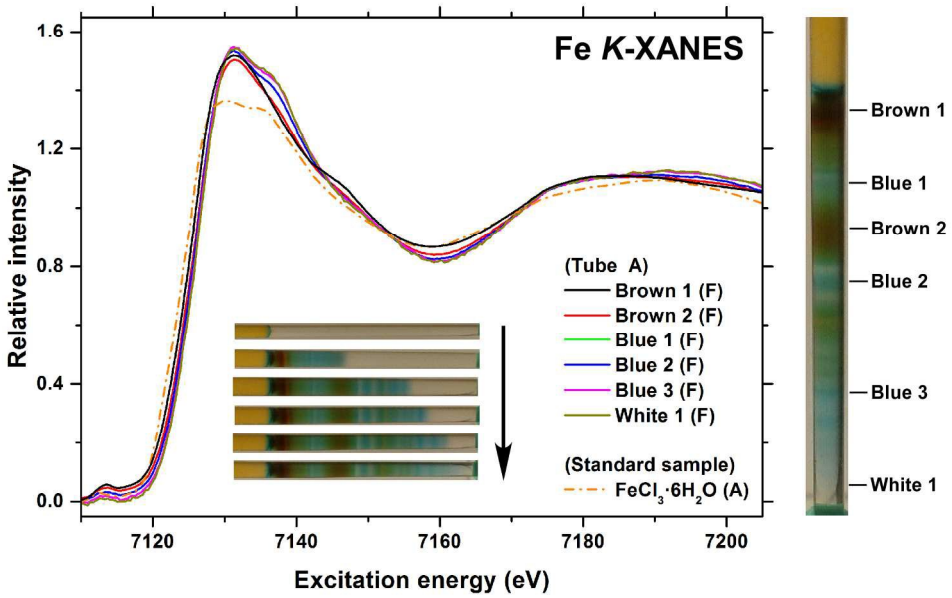

Journal of Analytical Atomic Spectrometry

ARTICLE

A Combined X-ray Spectroscopic Study on the Spontaneous Multicolored Pattern Formation in Gels Containing Iron(III) Chloride and Potassium Hexacyanoferrate(III)

Received 00th January 20xx,
Accepted 00th January 20xx

DOI: 10.1039/x0xx00000x

www.rsc.org/

Hisashi Hayashi*[a] and Hitoshi Abe[b,c]

We examined the potential of the combined use of two X-ray spectroscopic methods, time-resolved X-ray fluorescence (XRF) spectroscopy and position-dependent X-ray absorption near-edge structure (XANES) spectroscopy, for the study of intricate reaction-diffusion processes of inorganic compounds in gel media. To test this approach, we prepared a glass tube containing agarose gel mixed with $FeCl_3$ solution and water-glass gel mixed with $K_3[Fe(CN)_6]$ solution and hydrochloric acid. Wide brown and narrow blue bands formed in the water-glass gel, and the full development of the colored patterns took approximately 25 days. XRF and XANES spectroscopy were then used to study the time dependence of the Fe concentration distributions and the microscopic local structures of the Fe species formed in the colored bands, respectively. From these analyses, it was deduced that the brown bands were formed by the stable accumulation of Fe species whose local structure was mainly $[Fe(Cl)_2O_4]$; in contrast, the formation of the blue bands (originating from Prussian blue (PB) like compounds) was largely insensitive to both the Fe concentration distribution and the local structure of the dominant Fe species (mainly $[Fe(Cl)O_5]$) in the bands. Such insensitivities are attributable to the extremely small solubility product of PB ($\sim 10^{-41}$), which allows PB/PB-like compounds to form even under very low concentrations of both Fe^{2+} and $[Fe(CN)_6]^{3+}$. As a result, the brown bands were obscured by the blue colored PB-like compounds when high concentrations of Fe^{2+}, $[Fe(CN)_6]^{3+}$, and/or $[Fe(CN)_6]^{4+}$ were present, but became visible to reveal multicolored patterns under very low concentrations of these ions.

Introduction

Inorganic chemical reactions, coupled with diffusion of the formed species in gel media, can lead to the formation of intricate spatial patterns of precipitates.[1–3] A well-known example is Liesegang bands,[1,3,4] which are commonly observed in sedimentary rocks; they also form in gel media when one of the reagents, the inner electrolyte, is homogenized in the hydrogel, while the other, the outer electrolyte, penetrates the gel by diffusion. The two oppositely charged ions form precipitates when their concentrations exceed a threshold that is characterized by their solubility product constants. Thus, distinct precipitation bands periodically form behind the diffusion front of the outer electrolyte.[1–3] Such spontaneous pattern formation in reaction-diffusion (RD) systems has attracted the attention of chemists, physicists, and geologists for more than a century because it has been observed in many forms in different natural systems. In addition, the resultant structures are aesthetically appealing and have rich dynamics.[2,3] Furthermore, Grzybowski et al[2,5,6] recently developed experimental techniques that allow the initiation and control of RD processes in microgeometries, and this success has increased the interest in RD systems concerning micro- and nanotechnologies.

As Grzybowski has commented, there are still many hurdles to be overcome concerning the wider applications of RD processes.[2] A challenging but promising issue is parallel chemistry, in which multiple RD processes are encoded in parallel within the same system, realizing multiple experimental conditions within the same RD process.[2] For effective application of parallel chemistry in RD (e.g., for material fabrication), in addition to the details of the traditional systems,[7–9] more diverse and more intricate RD processes beyond simple Liesegang banding systems should be explored. Such investigations are currently progressing rapidly.[3,10–16]

In the study of the parallel chemistry of intricate RD processes (which generally include many elements), time dependence of the concentration distributions of each element and the chemical states of the locally formed species (which are often amorphous) are two indispensable pieces of information. However, acquisition of these data using conventional techniques which have been used in previous studies of Liesegang banding, such as FTIR,[9] XRD,[9] and UV-vis,[3,9,14] is difficult. Thus, we propose the combined use of two X-ray spectroscopic methods to study intricate RD processes in gels: in-situ time-resolved X-ray fluorescence (XRF) spectroscopy and position-dependent X-ray absorption near-edge structure (XANES) spectroscopy. These X-ray techniques, XRF[17] and

[a] Department of Chemical and Biological Sciences, Faculty of Science, Japan Women's University, 2-8-1 Mejirodai, Bunkyo, Tokyo 112-8681, Japan. E-mail: hayashih@fc.jwu.ac.jp
[b] Institute of Materials Structure Science, High Energy Accelerator Research Organization, 1-1 Oho, Tsukuba, Ibaraki 305-0801, Japan.
[c] Department of Materials Structure Science, School of High Energy Accelerator Science, SOKENDAI (the Graduate University for Advanced Studies), 1-1 Oho, Tsukuba, Ibaraki 305-0801, Japan.

XANES,[18] are non-destructive and element-selective. They require virtually no chemical pretreatment, and are applicable not only to the crystallites formed in gels (the main targets of previous Liesegang band studies) but also to amorphous species. Therefore, both during and after the RD processes, they can be used to monitor, in-situ, the concentration variations (XRF) and to study the microscopic local structures of chemical environment (XANES) of the element(s) of interest. Despite these merits, because X-ray spectroscopic techniques are unfamiliar to colloid and gel researchers, the two techniques have not been used significantly in the study of RD processes in gels; in particular, the combined use of time-resolved XRF and position-dependent XANES has not been investigated so far.

Experimental

Chemicals

Analytical reagent grade $K_3[Fe(CN)_6]$, $K_4[Fe(CN)_6]\cdot 3H_2O$, and $FeCl_3\cdot 6H_2O$ were obtained from Wako Pure Chemical Industries Ltd. (Chuo, Osaka) and were used without further purification. Hydrochloric acid (1.00 M), acetic acid (1.00 M), agar powder (400–600 g/cm² jelly strength), and sodium silicate solution (water-glass, 52–57% assay, 2.06–2.31 molar ratio of SiO_2/Na_2O) were also acquired from Wako Pure Chemical Industries Ltd. All aqueous solutions were prepared using deionized water.

Tube preparation

The glass tubes for the experiments, containing the inner and outer electrolyte gels, were prepared as follows: to prepare water-glass sols containing the inner electrolyte ($[Fe(CN)_6]^{3-}$ or $[Fe(CN)_6]^{4-}$), water-glass (1.6 g) was dissolved in deionized water (10 mL). The appropriate amounts of $K_3[Fe(CN)_6]$ or $K_4[Fe(CN)_6]\cdot 3H_2O$ were added to a further portion of deionized water (5 mL) to make $[Fe(CN)_6]^{3-}$ or $[Fe(CN)_6]^{4-}$ solutions (0.004–0.045 M). After dissolution of the powders, the two solutions were mixed, and either hydrochloric acid (16 mL, 0.53 M) or acetic acid (16 mL, 0.60 M) was added. This mixed solution (the water-glass sol) was continuously stirred for 5 min to allow homogenization, and transferred using a Pasteur pipette into quartz glass tubes with a length of 80 mm, an inner diameter of 3.5 mm, and a thickness of 0.010 mm (Mark-tube, Hilgenberg GmbH, Malsfeld). The sol solidified to a gel in the glass tube within 10 min.

To prepare the agarose sols containing the outer electrolyte ($[Fe^{3+}]$), firstly, an agarose sol of 2 w/w% was prepared by adding agar powder to deionized water (20 mL). Then, the appropriate amount of $FeCl_3\cdot 6H_2O$ was added to the agarose suspension, to obtain Fe^{3+} concentrations ranging from 0.15 M to 0.50 M. The mixture was heated at ~80 °C with continuous stirring until the agar dissolved (after a few minutes). The resulting sol was immediately poured, while hot, over the solidified water-glass gel in the glass tubes using a Pasteur pipette. The glass tubes were then covered with Parafilm and stored in a cooling chamber at 7 °C for 5 min to solidify the gels completely. In some experiments, instead of hot agarose sols, $FeCl_3$ aqueous solutions (without agarose) were poured directly above the water-glass gel in the tubes. The conditions for the tubes used in the experiments are summarized in Table 1. The resulting tubes were mounted on handmade sample holders (acrylic resin; 80 × 30 × 10 mm (h × w × d)), which had graduations for height and width in millimeters in order to allow for easy identification of band positions in the gels and easy transitions between band monitoring and XRF/XANES measurements.

Monitoring the evolution of multicolored bands

After the addition of the outer electrolyte sol/solution over the water-glass gel, the electrolyte components in both gels were capable of diffusing to the opposite side to react with each other. Blue and brown bands started to form near the junction, as shown in the results and discussion. The evolution of the colored bands was recorded for up to 40 days using a digital camera at room temperature (~20 °C), with intermittent in-situ XRF measurements also being performed. The Fe *K*-edge XANES spectra of the fully developed bands (i.e., once there were no more changes over time) were also measured. The tubes were found to be fully developed after ~550 h for tube A and ~900 h for tube F (see Table 1).

Table 1 Conditions for the experimental tubes: concentrations of agarose gel [agar] and water-glass gel [W.G.], initial concentrations of outer electrolyte $[Fe^{3+}]_0$, material of inner electrolyte (I.E.) and its initial concentration $[I.E.]_0$, and the acid material and its initial concentration $[acid]_0$.

Tube	[agar] %w/w	$[Fe^{3+}]_0$ (M)	[W.G.] %w/w	I.E.	$[I.E.]_0$ (M)	Acid	$[acid]_0$ (M)
A	2.0	0.15	30	$[Fe(CN)_6]^{3-}$	0.004	HCl	0.53
B	2.0	0.15	30	$[Fe(CN)_6]^{3-}$	0.004	CH_3COOH	0.60
C	0	0.15	30	$[Fe(CN)_6]^{3-}$	0.004	HCl	0.53
D	2.0	0.25	30	$[Fe(CN)_6]^{3-}$	0.045	CH_3COOH	0.60
E	2.0	0.50	30	$[Fe(CN)_6]^{3-}$	0.005	CH_3COOH	0.60
F	2.0	0.25	30	$[Fe(CN)_6]^{4-}$	0.025	CH_3COOH	0.60

Laboratory in-situ time-resolved XRF measurements

Details of the laboratory in-situ XRF setup employed have been previously described.[19] Briefly, an 18 kW X-ray generator (Rigaku, RU-300) with a Cu target was used for excitation and was operated at 200 mA and 40 kV. The X-rays from the generator were monochromated to give only Cu $K\alpha_1$ radiation and focused to ~0.5 mm in the horizontal direction by a SiO_2 Johansson-type crystal. The divergence of X-rays in the vertical direction was limited by a handmade collimator with a ~0.5 mm slit. The resultant beam size on the sample was 0.8 × 0.5 mm (h × w). The tube containing the gel sample was mounted on the sample holder and placed on a computer-controlled *X*-*Z* stage (Kohzu Precision, XA05A-L2) and was moved in 1 mm steps in the *Z* direction to detect the Fe *K*α emission at each position using a silicon drift detector (Amptek, XR-100 T). The XRF signals were collected for 100 s at each point by a multichannel analyzer (MCA, Amptek, MCA8000A). Under these settings, the time required for collection of a complete XRF distribution measurement over ~50 mm of a sample tube was ~1.4 h. As shown in ref. 19, the counts for the XRF band (presently, the Fe *K*α band) and background components in the measured spectra were both integrated over 20 channels (corresponding to an energy width of 390 eV) using the MCA. After subtracting the integrated background from the integrated raw Fe signals, the obtained intensities were used to construct the Fe *K*α distribution for each sample tube.

Position-dependent Fe K-edge XANES measurements using synchrotron radiation

XANES spectra at the Fe *K*-edge were collected at the bending-magnet beamline BL-9C[20] of KEK-PF, High Energy Accelerator Research Organization, Tsukuba, Japan. The storage ring was operated at 2.5 GeV with a 450 mA current. A Si(111) double-crystal monochromator was used to produce monochromatic X-rays, the energy resolution of which was ~1.4 eV around the Fe *K*-edge (~7110 eV). The high-energy harmonics in the beams were removed by detuning the monochromator. The incident beams were then vertically focused using a Rh-coated, cylindrically bent mirror. The beam size at the sample position was 0.5 × 1.5 mm (h × w).

Tube A/F was mounted on the sample holder and placed on a computer-controlled *Z* stage (Chuo Precision Industrial, ALV-102-HP) to allow changes to be made to the measurement positions of the tube. Fe *K*-edge XANES spectra of the samples were collected at room temperature between 7000 and 7300 eV (~110 eV below and ~190 eV above the Fe *K*-edge, respectively). The energy steps of the incident X-rays were 0.35 and 1 eV in the XANES region (7076–7181 eV) and the structureless regions (7000–7076 eV; 7181–7300 eV), respectively. The measurements were carried out in fluorescence mode by setting a Lytle-type detector normal to the beam to minimize background scattering. The fluorescence signals were collected for 5–10 s at each incident energy. Under these settings, the typical accumulation time of a spectrum was ~1 h. For comparison, Fe *K*-edge XANES spectra of several standard compounds, $K_3[Fe(CN)_6]$, $K_4[Fe(CN)_6]\cdot 3H_2O$, and $FeCl_3\cdot 6H_2O$, were also measured over the incident energy range indicated above. The measurements of the standard samples were carried out also in absorption mode by using an ion chamber as a detector, in order to correct the self-absorption effects in fluorescence mode XANES.

After approximating the profile observed from 7000 to 7100 eV (the region before the Fe pre-edge) as a straight line and subtracting this background component, the XANES spectra obtained were normalized, based on the assumption that the average absorption coefficient of Fe compounds is virtually the same after the white line (i.e., in the spectral region 7250 to 7300 eV). These normalized XANES data were used to examine the chemical states of the Fe species in the gels. In order to simulate the observed XANES spectra, ab initio self-consistent real-space multiple scattering calculations were also carried out using the FEFF 8.02 code.[21,22]

Results and discussion

To test our combined XRF–XANES analysis of RD processes, a water-glass gel containing a solution of $[Fe(CN)_6]^{3-}$ (the inner electrode) was connected to an agarose gel containing a solution of Fe^{3+} ions (the outer electrode) in a glass tube, and their intricate RD processes were studied. Iron was chosen because of its rich chemistry and its ease of detection by X-ray spectroscopy. The gel medium of the outer electrode was agarose, which is a standard substance in studies of gel RD processes.[2,3] The gel medium of the inner electrode (which was irradiated by X-rays) was water-glass, used because of its high stability and tolerance to X-ray irradiation.

In the present system, the following two species were expected to be produced: (i) the green colored Fe^{3+}-$[Fe(CN)_6]^{3-}$ complex (so called Berlin green (BG)) and (ii) the rusty-brown colored precipitates of aquoiron(III) ions ($[Fe(H_2O)_6]^{3+}$), resulting from formation of brown precipitates such as $Fe_2O_3\cdot nH_2O$ in aqueous media. Furthermore, because of the use of agarose, additional chemical processes were expected. Agarose is comprised of alternating (1→3)-β-D-galactose and (1→4)-3,6-anhydro-α-L-galactose repeat units, and reducing sugars can form by hydrolysis during the heating process used to disperse the agarose gel. In the agarose gel, these reducing sugars can partially reduce the Fe^{3+} ions to Fe^{2+} forming a third iron species, Prussian blue (PB, ferric hexacyanoferrate with Fe^{3+} ions coordinated to nitrogen and Fe^{2+} ions coordinated to carbon, $Fe^{III}_4[Fe^{II}(CN)_6]_3$).[23] Because the solubility product constant of PB is very small (3×10^{-41}), even small amounts of Fe^{2+} can form PB and/or PB-like compounds in the gel. Thus, this Fe system can form multicolored precipitate/complex bands, including BG (green), aquoiron(III)-related precipitates (brown), and PB or PB-like compounds (blue). Although multicolored bands of the present system have not been previously reported, in our experiments the expected multicolored patterns were observed.

Macroscopic Dynamics

The change of color, from light yellow (due to $K_3[Fe(CN)_6]$) to blue, took place at the junction seconds after pouring the agarose sol onto the water-glass gel. The observed blue color indicates the formation of PB, suggesting that the Fe^{3+} ions are

partially reduced to Fe^{2+} in the agarose sol, as expected. Here, we describe the macroscopic evolution of the colored patterns.

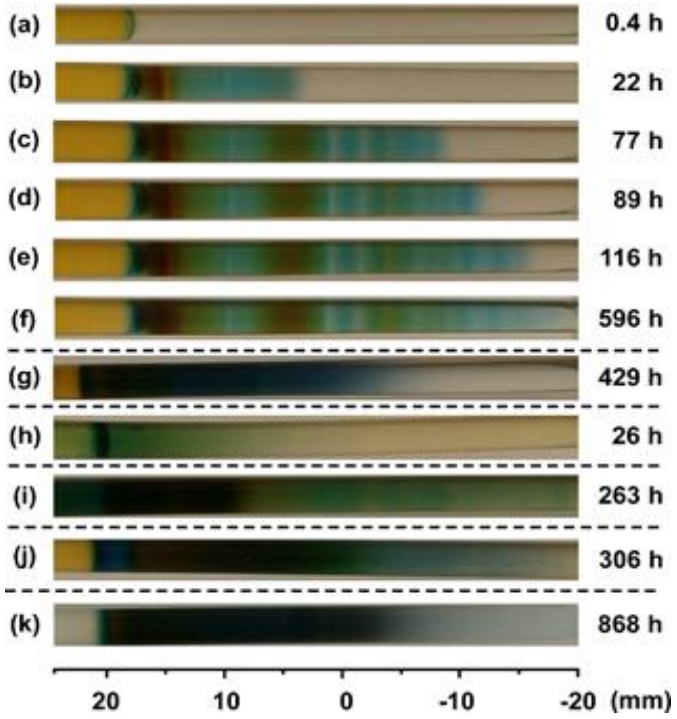

Fig. 1 (a)–(f) The spatiotemporal evolution of the colored bands in tube A. Snapshots were taken at varying times after the addition of the outer electrolyte, as indicated at the right side of each picture. For comparison, snapshots of the gel samples prepared under different conditions are also shown. Pictures (g), (h), (i), (j), and (k) were obtained from tube B at 429 h, tube C at 26 h, tube D at 263 h, tube E at 306 h, and tube F at 868 h, respectively.

Figs. 1(a)–(f) show the spatiotemporal evolution of the colored bands formed in the tube labeled A in Table 1. In the agarose gel (on the left side of Fig. 1), the deep yellow color was maintained with almost no loss of intensity over the observation period of ~40 days. In contrast, the following changes were observed in the water-glass gel (right side in Fig. 1): initially, the blue band near the gel junction propagated downwards through the tube (to the right side of the figure). After ~20 h, when the band had propagated to a distance of ~13 mm from the junction, it split, giving rise to new, closely separated bands. At this time, the color of the bands that formed near the junction changed from blue to brown, as shown in Fig. 1(b). Up to ~80 h after the addition of the outer electrolyte, the diffusion front continued to move down the tube, leaving behind relatively broad (~5 mm) brown bands and relatively narrow (~2 mm) blue bands (Fig. 1(c)). The brown and blue bands suggest the existence of aquoiron(III)-related compounds and PB-like ones, respectively, in each region. As the diffusion front reached ~70% of the length of the tube (Figs. 1(c) and 1(d)), a third hazy-brown region at around $Z = -4$ mm started to form, overlapping the blue bands. With time, the third brown band broadened and the diffusion front moved further, as shown in Fig. 1(e). The diffusive motions and the color changes in tube A (as well as in the other tubes referred in Table 1) became less noticeable after ~170 h, and virtually stopped after ~360 h. Fig. 1(f) shows the fully-developed bands in tube A, which were obtained after ~596 h (~25 days). Over the observation period of ~40 days, both the brown and blue bands that had formed appeared to be almost static after the propagating diffusion front had passed, and, once formed, the locations of their centers of gravity did not change.

The formation of multicolored bands, as shown in Figs. 1(b)–(f), was only observed under a rather limited set of preparation conditions. For example, the use of acetic acid instead of hydrochloric acid (tube B in Table 1, acting as control experiment 1 for tube A) did not lead to evenly separated bands when other conditions (including the concentrations of the electrolytes) were the same. In the water-glass gel of tube B, only a diffuse blue-colored region was observed after ~18 days (Fig. 1(g)). In the system without agarose sol in the outer electrolyte (tube C in Table 1, Fig. 1(h), control experiment 2 for tube A), a hazy green color (possibly BG) was observed instead of a blue region. As expected, the concentration of both outer and inner electrolytes can also change the morphology of the bands in the water-glass gel. For example, the tube with agarose gel mixed with 0.25 M $FeCl_3$ solution and water-glass gel mixed with 0.045 M $K_3[Fe(CN)_6]$ solution and 0.6 M acetic acid (tube D in Table 1, control experiment 3) also resulted in brown and blue regions (Fig. 1(i)), but the widths of the bands were rather broad and the bands overlapped, unlike those seen in the case of tube A. Furthermore, the tube containing agarose gel mixed with 0.50 M $FeCl_3$ solution and water-glass gel mixed with 0.005 M $K_3[Fe(CN)_6]$ solution and 0.6 M acetic acid (tube E in Table 1, control experiment 4) did not show these relatively sharp colored bands (Fig. 1(j)).

For comparison, Fig. 1(k) shows the results for an almost single-colored Fe system (tube F in Table 1, control experiment 5), rather than a multicolored system. Tube F contained agarose gel mixed with 0.25 M $FeCl_3$ solution (the same as tube D) and water-glass gel mixed with 0.025 M $K_4[Fe(CN)_6]$ solution and 0.6 M acetic acid (again, the same as tube D). This tube was expected to form PB and, in fact, a broad blue band was formed up to ~170 h. Fig. 1(k) is a snapshot of its fully-developed pattern at 868 h. Although a faint, narrow brown band was found at just below the junction (~19.5 mm) at 868 h, the color of the majority of the continuous band ranging from 18 to -5 mm was dark blue.

These observations indicate that the Cl^- ions played a key role in the formation of the brown bands. In fact, when we used acetic acid instead of hydrochloric acid (tube B), no brown band appeared when all other conditions were the same. In order to form brown bands when using acetic acid, a higher concentration of $FeCl_3$ was required: either 0.25 M (tubes D and F) or 0.50 M (tube E). The role of Cl^- ions will be discussed further using position-dependent XANES results.

It is well known that Liesegang patterns vary with changes in the concentration of the reactants.[1,24,25] For example,

systematic studies by Ross et al. on a $Pb(NO_3)_2$ and KI system in agar gels indicated that the PbI_2 precipitation patterns, characterized by the band number N, the band location x_n, and the band width Δw_n, strongly depended on the initial concentration difference of the two electrolytes, Δ, and the initial ion products of the electrolytes, σ.[24,25] The well-known spacing law of Liesegang bands, x_{n+1}/x_n = constant,[2,3] is obeyed only when σ and Δ are large (and consequently, N is also large).[24] When σ is varied but Δ is fixed, the bands broaden as σ decreases.[24] When Δ is varied at constant σ, the location of bands varies with Δ in a complicated manner.[24] When both σ and Δ are small, the precipitation patterns are increasingly stochastic, in terms of both the probability of band formation and the reproducibility of the band location.[25]

The results of tube A (Fig. 1(a)–(f)), including (1) the broadness of both the brown and blue bands, (2) the absence of any indication of the spacing law of Liesegang bands, and (3) the stochastic property on the band positions, correspond fairly well with the above results for the stochastic variations of Liesegang bands when both σ and Δ are small. Regarding the blue bands, because the concentrations of $K_3[Fe(CN)_6]$ (initially 0.004 M) and the minor, reduced iron species (Fe^{2+}) in tube A must both be rather low, both Δ and σ must be relatively small; therefore, the observed broad and stochastic features of the blue bands are to be expected. Meanwhile, attention should also be paid to the differences between the conventional stochastic Liesegang patterns and the observed blue patterns: the band shapes are simple rather than complicated, and N is relatively large (>8). The reasons for these differences are not clear. Regarding the brown bands (possibly due to compounds including aquoiron(III) ions), no theory is currently available, even for qualitative interpretation of the pattern formation. The X-ray spectroscopic results of this poorly-understood, multicolored RD system are shown and discussed in the following sections.

Time-resolved Fe *Kα* intensity distributions

Fig. 2(a) shows the time dependence of the Fe *Kα* intensity distributions for tube A. XRF measurements were performed at varying times after the addition of the outer electrolyte, as indicated for each intensity distribution. The vertical and horizontal axes in Fig. 2 are the count rate of the integrated Fe *Kα* signals and the relative positions of the incident X-rays on the sample tube, respectively. The Fe *Kα* distributions for the "bottom" region of the tube (the right side of the figure, from 5 to −20 mm of the relative position) are shown in enlarged scale in the inset. To allow comparison of the Fe *Kα* intensity distributions with the positions of the colored bands, the snapshot obtained at 596 h (as in Fig. 1(f)) is also displayed at the top of Fig. 2(a).

The observed Fe *Kα* intensity distributions changed markedly over time, in accordance with the macroscopic evolution of the colored bands (Fig. 1). Immediately after initiation (0.4 h), the Fe *Kα* intensity distribution formed a clear threshold at the junction of the gels, indicating that, at this time, Fe diffusion from the agarose gel to the water-glass gel was minimal. After ~3 h, the slope of the distribution curve became rather gentle, suggesting

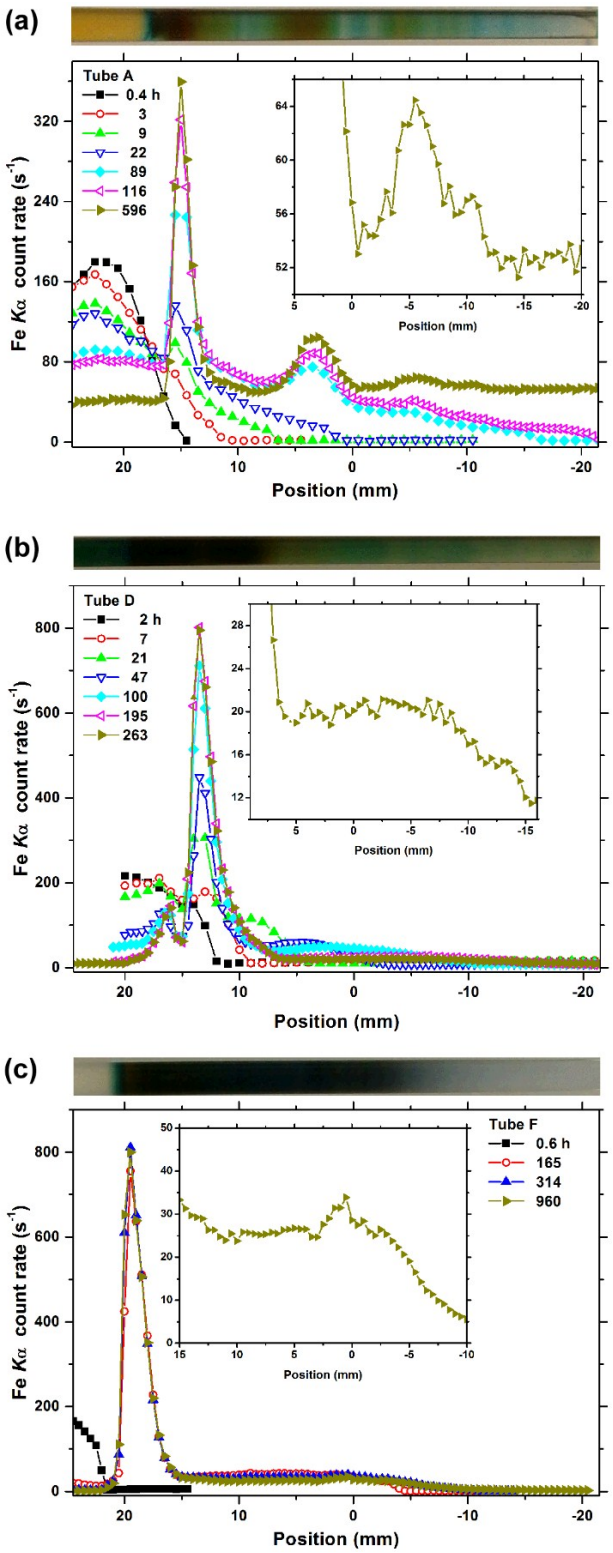

Fig. 2 Time dependences of Fe *Kα* intensity distributions in (a) tube A, (b) tube D, and (c) tube F. XRF data were recorded at varying times after the addition of outer electrolyte, as indicated for each distribution. Insets: the XRF distributions shown in enlarged scales for "bottom" region of the glass tubes. For comparison of the XRF intensity distributions with the positions of colored bands, the snapshots in tube A at 596 h (Fig. 1(f)), tube D at 263 h (Fig. 1(i)), and tube F at 868 h (Fig. 1(k)) are also displayed at the top of Figs. 2(a), 2(b), and 2(c), respectively.

the progress of Fe diffusion. After ~9 h, a peak in the Fe *K*α intensity at the junction was observed. This increase in the intensity (caused by the accumulation of Fe species) continued up to ~600 h after the addition, along with the deepening of the brown color in the corresponding region. Additionally, up to ~100 h after the addition, the threshold of the Fe *K*α intensity continued to shift downward, with a position that approximately agrees with the front of blue region in the glass tube. After the threshold reached the bottom of the glass tube, the Fe *K*α intensities in the water-glass gel approximately continued to gradually increase up to ~600 h.

After ~70 h, a broad peak appeared at around 4 mm. Furthermore, after ~110 h, another weak peak emerged around −6 mm (its fully-developed profile at 596 h is shown in the inset of Fig. 2(a)). The positions of both these XRF peaks agreed with those of the brown bands, strongly suggesting that these were composed of concentrated Fe species.

The peaks in the Fe *K*α distribution at 15, 4, and −6 mm were static, suggesting that the factors driving accumulation of Fe species were rather stable. The intensities of the peaks increased monotonically with time and occurred without oscillations that would imply intricate precipitation and re-dissolution processes, as have been observed elsewhere.[3,9,11,13] These results suggest that Fe accumulation in the brown regions was subject to processes that are both simple and repetitive.

In contrast, the correspondence between the positions of blue bands and the Fe *K*α distribution is not clear. No characteristic peak structures were observed within the blue region, beyond statistical uncertainty, as can be seen by comparison of the snapshot of tube A with the enlarged Fe *K*α distribution in the inset. This finding means that the concentration of Fe species forming the blue bands is low, and that the main Fe components in the blue regions are not visible by eye, as are the components in the colorless regions in the "aged" samples (e.g., tube A after 596 h, Fig. 1(f)). Since PB/PB-like compounds are expected to be responsible for the blue color, the low concentration of blue colored species is consistent with a rather low initial concentration of $K_3[Fe(CN)_6]$, as well as the fact that Fe^{2+} ions are the minor component in tube A.

For comparison, the time dependence of the Fe *K*α intensity distributions for tubes D and F are shown in Figs. 2(b) and 2(c), with the snapshots obtained at 263 h (tube D as seen in Fig. 1(i)) and at 868 h (tube F as seen in Fig. 1(k)) displayed at the top of the figures.

A peak started to form in tube D somewhat below the gel junction (12.5 mm) at a relatively early stage (7 h), and grew with time without changing its position. The peak intensity was 2.2 times larger than the corresponding peak in tube A, reflecting the higher concentrations of both the outer and inner electrolytes. In common with tube A, the threshold of the Fe *K*α intensity shifted down the tube with time.

Although the initial concentration of $K_3[Fe(CN)_6]$ in tube D was ~10 times higher than that in tube A, the positions of the (rather broad) blue bands showed no apparent correspondence with the Fe *K*α distribution. This result supports our supposition that in tubes A–E (where the initial concentration of $K_3[Fe(CN)_6]$ was less than 0.045 M), the amounts of Fe species responsible for the blue bands were relatively small, and "(almost) invisible" Fe species dominated the contribution to the Fe *K*α intensities in the blue regions.

Although there are some similarities in the Fe *K*α distributions of tubes A and D, there are also several differences. Firstly, note that with the exception of the junction peak, peak structures were not observed in the water-glass gel of tube D. Consistent with this XRF result, no additional brown regions were found below the junction in tube D. Thus, contrary to the case of the blue bands, the close relationship between the brown bands and the Fe *K*α distribution peaks (or locally concentrated Fe species) can be confirmed.

Secondly, it is also interesting that a second XRF peak became apparent above the junction (17 mm) after ~21 h, suggesting the accumulation of Fe species in the agarose gel that may be due to some "backward flow" of the inner electrolyte to the upper gel. The color of the region forming the two peaks was dark brown, and, although the peaks are quite distinct in XRF distributions, they were difficult to distinguish visually. The discovery of this "hidden" region of Fe accumulation demonstrates the potential of using XRF for the in-depth analysis of metal-ion distributions in gels.

As shown in Fig. 2(c), the Fe *K*α intensity distribution profiles in tube F were overall similar to those for tube D: a peak formed somewhat below the gel junction (~19.5 mm), and grew with time without changing its position. The position of this strong peak corresponded to the faint, narrow brown region, again confirming the close relationship between the brown band and the Fe *K*α distribution peak. The peak intensity was also similar to that in tube D, reflecting the fact that the concentration of the major Fe source was the same (Fe^{3+}, 0.25 M). As was the case for tubes A and D, the threshold of the Fe *K*α intensity distribution shifted down the tube with time.

Interestingly, unlike for tubes A and D, the distribution of the broad blue band in tube F showed some correspondence with the Fe *K*α distribution, although it is not very apparent. For example, the blue band became diffuse below approximately -4 mm, and the Fe *K*α intensity decreased from this position (see inset of Fig. 2(c)). This result suggests that the amount of Fe species in tube F was at least partially responsible for the blue (possibly PB-like) bands, as expected.

From these XRF results, the Fe concentration dependence of the brown bands was clarified: (1) the brown bands formed due to the presence of concentrated Fe species in the water-glass gel, and (2) the factors driving the accumulation of the Fe species were relatively stable.

In contrast, the blue bands (partially) depend on the Fe concentration in the gels for the $Fe^{3+}/[Fe(CN)_6]^{4+}$ system, but not for the $Fe^{3+}/[Fe(CN)_6]^{3+}$ system. This could be due to the very small solubility product constants of PB species; i.e., even though the colorless Fe species were dominant in the blue and white regions, and the concentrations of Fe^{2+} and/or $[Fe(CN)_6]^{3+}$ ions were low (tubes A, B, D, and E), the PB-like compounds could form, preventing the Liesegang band-like formation of discrete blue bands observable by eye. Thus, the Liesegang band-like patterns, as observed in tube A, were limited to cases where concentrations of both Fe^{2+} ions and $[Fe(CN)_6]^{3+}$ were very low (or,

where both σ and Δ were very small); if not, a continuous band emerged, as was the case for tubes B–F. Detailed determination of the boundary conditions of σ and Δ required to yield the Liesegang band-like pattern will be an interesting piece of future work.

Position-dependent Fe K-edge XANES spectra

After examining the macroscopic evolution of the gel systems by XRF, the microscopic local structures of the Fe compounds in the fully-developed bands of tubes A and F were explored by XANES.

Fe *K*-edge XANES spectra have already been measured for a wide range of materials,[26–28] including hexacyanide complexes[29] and aqueous $FeCl_3$ solutions.[30] Furthermore, site-selective extended X-ray absorption fine structure (EXAFS) spectra of PB have been measured.[31] XANES measurements of Fe gel systems including RD processes are, however, rather scarce.[32] In this study, we focused mainly on the main-edge structures, but weak pre-edge structures are also discussed.

The Fe *K*-edge XANES spectra of $FeCl_3{\cdot}6H_2O$, $K_3[Fe(CN)_6]$, and $K_4[Fe(CN)_6]{\cdot}3H_2O$, which were obtained in absorption mode and denoted "A", are plotted in Fig. 3(a). The observed profiles agree well with those in refs. 26, 29, and 30. The XANES profiles of $K_3[Fe(CN)_6]$ and $K_4[Fe(CN)_6]{\cdot}3H_2O$, where Fe^{3+} and Fe^{2+} ions, respectively, have strong bonds with six CN^- ions in O_h symmetry, are fairly similar, reflecting the strong similarity of their local atomic structures (although small peak shifts were observed in the main and subsequent peaks, depending on the Fe oxidation state).[29] Their intense, narrow main peak can be attributed to the transition of the *K* electron to the t_{1u}* orbital of a simple molecular orbital (MO) model.[26] In the multiple scattering model, both the first and the second peak can be interpreted as the shape resonance of the CN groups, within which the excited *K* electron is vertically trapped.[29]

In contrast, the XANES profile of $FeCl_3{\cdot}6H_2O$, where Fe^{3+} ions have weak bonds with four H_2O molecules and two Cl atoms in octahedral geometry (corresponding to *trans*-$[FeCl_2(H_2O)_4]^+$)[30] is clearly different from the two hexacyanide profiles. The main peak appears to have two components, which can be assigned to absorption into the e_{1g}* and t_{2g}* orbitals using a simple MO model.[26] In aqueous $FeCl_3$ solutions, the relative intensity of the two components changed with $FeCl_3$ concentration; for low concentrations (<1 M), the first component became dominant, forming a relatively sharp peak; in contrast, at high concentrations (>3 M) the second component became comparable in intensity to the first, forming a broad doublet band, as in the case of $FeCl_3{\cdot}6H_2O$.[30] Thus, the Fe *K*-edge XANES shows characteristic features for both hexacyanide-related compounds (including PB) and aquoiron(III)-related species; therefore, the technique is useful for the determination of the dominance of these two compounds within a measured area.

When applying the XANES technique to samples such as those used in this study, it is important to consider the self-absorption effect. Because the samples were too thick (3.5 mm) to measure XANES in absorption mode, fluorescence detection was required. For XANES measurements in fluorescence mode, self-absorption by absorbing atoms can attenuate strong peaks

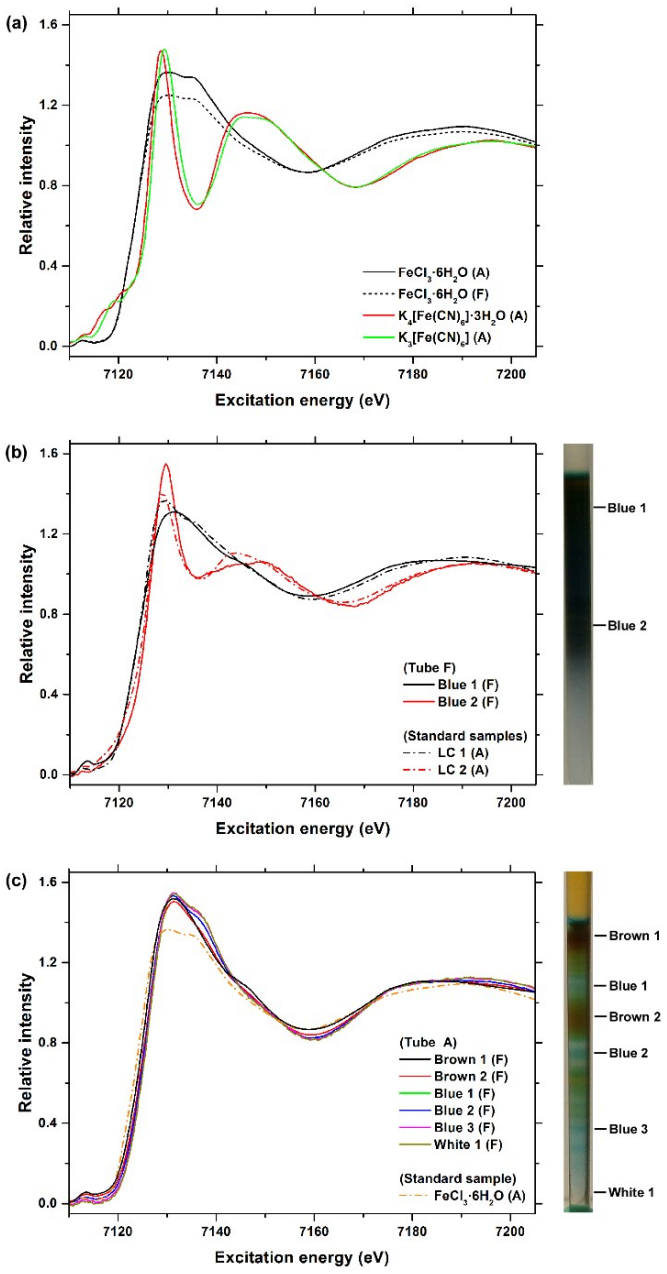

Fig. 3 (a) The Fe *K*-edge XANES spectra of $FeCl_3{\cdot}6H_2O$, $K_3[Fe(CN)_6]$, and $K_4[Fe(CN)_6]{\cdot}3H_2O$, and the positions at which the Fe *K*-edge XANES spectra were measured in (b) tube F and (c) tube A. The sampling positions, with labels such as "blue 1" and "brown 1", are indicated by bars on the snapshots at the right side of each figure. The snapshots were taken at 868 h (tube F) and 596 h (tube A). The labels "A" and "F" indicate the measurement mode of XANES: absorption mode and fluorescence mode, respectively. In Fig. 3(b), the linear combination of the spectra of the standard samples, "LC 1" and "LC 2", are also shown.

in the XANES profile (particularly for its white line) when the penetration depth into the sample is dominated by the absorbing atoms. This is called the self-absorption effect. In order to show the self-absorption effect for $FeCl_3{\cdot}6H_2O$, the XANES spectrum of $FeCl_3{\cdot}6H_2O$ obtained in fluorescence mode is also plotted in Fig. 3(a). The attenuation of the white line by

the self-absorption effect is clear, with a reduction of ~8%. We deduced the ratio of the two $FeCl_3 \cdot 6H_2O$ spectra at each excitation energy, and used this to correct for the self-absorption effect as follows. First, the self-absorption correction factors were estimated from the obtained ratio, under the following assumptions: (i) the excitation-energy dependence of the self-absorption effect for the samples was the same as that for $FeCl_3 \cdot 6H_2O$, and (ii) the magnitude of the effect was proportional to the Fe $K\alpha$ intensity at an excitation energy of 7131 eV (the white line energy of $FeCl_3 \cdot 6H_2O$). Then, the measured fluorescence-mode XANES spectra were multiplied by the estimated factors, unless the Fe $K\alpha$ intensity at 7131 eV of the samples was less than 10% of that of $FeCl_3 \cdot 6H_2O$. This cutoff was used because in such dilute samples the self-absorption effect was considered to be almost negligible (<0.8%). As a result, the self-absorption correction was conducted only for the XANES spectra obtained at the three sampling positions: "blue 1" in Fig. 3(b), and "brown 1" and "brown 2" in Fig. 3(c).

We first examined the XANES of an almost single-colored Fe system, tube F. The Fe *K*-edge XANES spectra of tube F, shown in Fig. 3(b), were obtained in fluorescence mode at two sampling positions, labeled "blue 1" (near the gel junction) and "blue 2" (the blue region at the lower part of the tube). The positions are indicated by bars on the snapshots in the right side of the figure. Although the color of tube F seems to be similar at both positions, the XANES spectra were distinctly different. Concerning the peak positions and peak widths, the XANES at blue 2 is in fairly good agreement with the XANES of $[Fe(CN)_6]$ compounds, although there are significant differences in their relative peak heights. In contrast, the XANES at blue 1 qualitatively agrees with the XANES of $FeCl_3 \cdot 6H_2O$, which suggests that aquoiron(III)-related compounds were dominant at this position.

The two XANES spectra were analyzed by linear combination (LC) of the spectra of the standard samples shown in Fig. 3(a) by trial and error. "LC 1" and "LC 2" are the best-fit results for blue 1 and blue 2, respectively. In LC 1, the ratio of $FeCl_3 \cdot 6H_2O$ to the the averaged hexacyanide spectrum (the model for PB; $0.5 \times K_3[Fe(CN)_6] + 0.5 \times K_4[Fe(CN)_6] \cdot 3H_2O$) was 0.88 : 0.12 = 22 : 3, while in LC 2 it was 0.45 : 0.55 = 9 : 11. Although not perfect, these LC profiles resulted in fairly good reproductions of the measured XANES spectra. This result suggests that hexacyanide- (or PB-) related compounds were dominant at blue 2, which is consistent with the correspondence between the blue color and the Fe $K\alpha$ intensity observed in Fig. 2(c). In contrast, the $FeCl_3 \cdot 6H_2O$-like aquoiron(III)-related compounds were suggested to be dominant at blue 1, although the blue color resulting from the PB-related compounds prevents identification of the differences in the local Fe structures by eye.

Fig. 3(c) shows the Fe *K*-edge XANES spectra of the main target of the investigation, tube A, which were recorded at the sampling positions indicated by bars on the snapshot at the right side of the figure. While distinctive colors (the brown and blue bands, as well as white background) can be seen in tube A by eye, these variations are not necessarily reflected in the XANES profiles. As is evident from Fig. 3(c), all of the XANES spectra obtained in tube A were similar and qualitatively agree with the $FeCl_3 \cdot 6H_2O$ spectrum. These findings indicate that (1) the local structure around the Fe atoms in tube A was similar at all measured positions, and (2) the Fe atoms were mainly surrounded not by CN^- but by O and Cl^- in a (distorted) octahedral geometry (i.e., the dominant Fe species were aquoiron(III)-related compounds, as was the case for blue 1 in tube F). The fact that there is very little difference in XANES spectra between the blue regions (blue 1 to blue 3) and the white (background) region (white 1) implies that the blue color was independent of the local structure around Fe of the main compounds, again as was the case of tube F.

Despite their overall similarity, the XANES spectra obtained from the two brown regions are noticeably different from the others, especially the relatively low intensity of the high-energy hump at ~7137 eV. This suggests that the local structure of the dominant species in the brown bands is slightly, but not insignificantly, different from the structures of the Fe species formed in the blue/white bands. It is also worth noting that the XANES spectra of tube A are not quantitatively the same as the spectrum of $FeCl_3 \cdot 6H_2O$: for example, the relative intensity of the main peak at 7131 eV of brown 1 is still noticeably stronger than that of $FeCl_3 \cdot 6H_2O$. LC trials using the $FeCl_3 \cdot 6H_2O$ and the averaged hexacyanide spectra failed to reproduce the XANES spectra obtained from tube A: for example, such LC profiles resulted in considerable underestimation of the main peak at 7131 eV, because the intensity of the tube A spectra at 7131 eV (~1.5) was stronger than in the $FeCl_3 \cdot 6H_2O$ spectrum (~1.4) and the averaged hexacyanide spectrum (~1.1). The profile analysis of the tube A XANES spectra will be performed using FEFF simulation in the following section.

Here let us discuss the pre-edge structures of the measured spectra, although their relatively weak signal intensities hindered detailed analysis. The pre-edge structures in *K*-edge absorption spectra of transition metal compounds can be assigned to quadrupole transitions from the 1s core state to the empty 3d state; if the inversion symmetry of ligand geometry around the metal is broken, the pre-edge components gain additional intensity due to the local mixing of the 3d and 4p wavefunctions, allowing dipole transitions to the 4p character of the 3d band.[27,33] The pre-edge structures also can yield information on the oxidation states and geometry of the Fe atoms.[27,28,30,34]

In Figs. 4(a) and 4(b), the pre-edge profiles observed below 7125 eV in Fig. 3(b) and 3(c) are re-plotted with an expanded scale. The profiles of $FeCl_3 \cdot 6H_2O$, $K_3[Fe(CN)_6]$, and $K_4[Fe(CN)_6] \cdot 3H_2O$ also shown in Fig. 4 essentially agree with those reported in refs. 27 and 30 (the fine structure in the pre-edge bands[33,34] is considered to be smeared out because of the resolution of the instrument (~1.4 eV)).

While the main-edge profiles of $K_3[Fe(CN)_6]$ and $K_4[Fe(CN)_6] \cdot 3H_2O$ are fairly similar (Fig. 3(a)), the pre-edge profiles (Fig. 4(a)) are rather different from each other, depending on the oxidation state of Fe. Fig. 4(a) also clearly shows that the pre-edge profile of $FeCl_3 \cdot 6H_2O$ is different from these hexacyanide profiles, with a noticeable band at ~7113 eV and almost no distinctive structure around 7118 eV. These

features are characteristic of Fe^{3+} complexes of H_2O and Cl with octahedral geometry.[27,30]

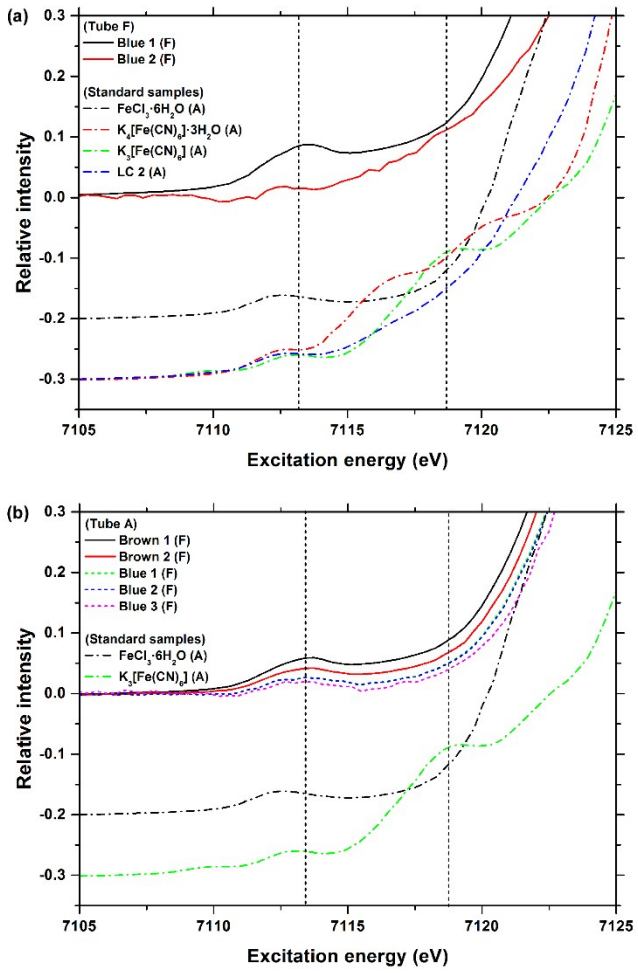

Fig. 4 Position dependences of the Fe pre-edge spectra in (a) tube F and (b) tube A. For comparison, the pre-edge spectra of $FeCl_3·6H_2O$, $K_3[Fe(CN)_6]$, $K_4[Fe(CN)_6]·3H_2O$, and "LC 2" from Fig. 3(b) are also re-plotted. The labels, "A" and "F", indicate the measurement mode of XANES: absorption mode and fluorescence mode, respectively. The vertical dotted lines serve as a guide to the eye.

As was the case for the main edge results, the LC 2 profile reproduced the overall shape of the pre-edge spectrum of blue 2 of tube F fairly well (Fig. 4(a)). In the LC 2 profile, the peak structures of the two hexacyanides in the region of 7113–7123 eV canceled each other out due to their superposition. Since PB is a mixed-valence compound of Fe^{2+} and Fe^{3+}, the observed agreements between the blue 2 and LC 2 pre-edge profiles confirmed the dominance of PB-like compounds in the blue 2 region.

In contrast, the pre-edge profiles at blue 1 in tube F and at brown 1, brown 2, blue 1, blue 2, and blue 3 in tube A are similar to the $FeCl_3·6H_2O$ profile. This similarity suggests the dominance of the Fe^{3+} species surrounded by H_2O and Cl with octahedral geometry in the above regions, which is again consistent with the main-edge results shown in Fig. 3.

The XANES results shown in Figs. 3 and 4 suggest that several advanced XANES techniques are applicable to the study of RD processes in gels. Because the dynamics of RD processes in gels is slow and the acquisition time to obtain one XANES spectrum was approximately 1 h, time-resolved, position-dependent XANES measurements are, in principle at least, possible, although relatively long, rather flexible machine time would be required at a synchrotron radiation facility. In addition, the signal intensity in the pre-edge region seemed to be tolerable for high-resolution XRF detection, if ~5× longer acquisition times were secured or ~5× more intense X-ray sources were available. Thus, if these requirements are fulfilled and a high-resolution emission spectrometer[35,36] can be introduced into a beamline, several advanced, high-resolution XANES techniques, including lifetime-broadening-suppressed, high-resolution pre-edge measurements,[31,35–37] and self-absorption-free, high-resolution XANES measurements[37,38] could also be applied. These techniques should be examined in future work.

FEFF simulation of XANES spectra

In order to provide a greater understanding of the XANES of tube A, we conducted preliminary FEFF calculations using small, simple clusters. More detailed analysis using larger, more intricate clusters has not currently been attempted, because the complicated nature of the samples means their exact compositions are unknown. In the FEFF calculations, we employed a distorted octahedral cluster, where an iron atom was in the center and the bond angle was fixed at 90°. The maximum value for overlapping muffin-tins and the radius of cluster for full multiple scattering were 0.12 and 0.35 nm, respectively. The bond distances of Fe–Cl and Fe–O and the coordination numbers of the calculated clusters are shown in Table 2, where the bond lengths employed and the corresponding Fe^{3+} concentrations in aqueous solutions were taken from ref. 30.

Table 2 Bond lengths of Fe–Cl and Fe–O and the coordination numbers (Coord. num.) for calculated clusters: the corresponding Fe^{3+} concentrations (Fe^{3+} conc.) in aqueous solutions[30] are also shown.

Symbols	Fe^{3+} conc. (M)	Coord. num. Cl	Coord. num. O	Fe–Cl (nm)	Fe–O (nm)
$FeCl_3$	–	2	4	0.230	0.206
4MT	4.3	2	4	0.230	0.202
4MC	4.3	2	4	0.230	0.202
0.7M	0.74	1	5	0.228	0.200
0.1M	0.14	1	5	0.235	0.199
Aqua	0	0	6	–	0.200
SB	–	2	4	0.230	0.190

Fig. 5(a) shows Fe *K*-edge XANES profiles computed by the FEFF 8.02 code for the clusters shown in Table 2. Here, "$FeCl_3$" and "4MT" clusters (as well as "SB" clusters) have two Cl atoms in *trans*-geometry, while "4MC" cluster has *cis*-geometry. The

"$FeCl_3$", "4MT", "0.7M", and "0.1M" clusters were the models of $FeCl_3 \cdot 6H_2O$, 4.3 M $FeCl_3$ aqueous solution, 0.74 M $FeCl_3$ aqueous solution, and 0.14 M $FeCl_3$ aqueous solution, respectively.[30] The "Aqua" cluster was the model for $[Fe(H_2O)_6]^{3+}$ ions in Fe^{3+} aqueous solutions. Interestingly, the calculated low-energy XANES (<7140 eV) for $[Fe(Cl)_2(O)_4]$ clusters ($FeCl_3$, 4MT, and 4MC) showed marked changes as the structure varied. In contrast, there was very little difference between the calculated profiles for the $[FeClO_5]$ clusters (0.7M and 0.1M). In addition, a systematic high-energy shift of the absorption edge was observed to increase substitution of Cl with O. The high-energy region of the calculated XANES profiles (>7150 eV) showed little differences among profiles.

In Fig. 5(a), the experimental XANES spectrum of $FeCl_3 \cdot 6H_2O$ has also been plotted. As expected, the theoretical "$FeCl_3$" profile quantitatively reproduced the experimental $FeCl_3 \cdot 6H_2O$ spectrum, except the pre-edge region where dipole-allowed, multiple scattering calculations are less accurate. This finding confirmed that FEFF simulations can be used for quantitative analysis of the main-edge structures of the present system.

In Fig. 5(b), the brown 1 spectrum is compared with the calculated profiles. For comparison, the $FeCl_3 \cdot 6H_2O$ spectrum is also shown. Fig. 5(b) indicates that the more intense white line of brown 1 is attributable to the longer Fe–O length of the $[Fe(Cl)_2(O)_4]$ structure in the gels, as suggested by 4MT and 4MC. The brown 1 spectrum was further analyzed by the linear combination of the 4MT and 4MC profiles by trial and error. "FEFF-LC 1" is the best-fit result for brown 1, and consisted of 0.60 of 4MT and 0.40 of 4MC, giving a good reproduction of the brown 1 spectrum. This strongly suggests that Fe species with the local structures of $[Fe(Cl)_2O_4]$ with bond lengths similar to concentrated (~4 M) $FeCl_3$ solutions, were dominant in brown 1.

In Fig. 5(c), the blue 3 spectrum is compared with the calculated profiles. For comparison, the brown 1 spectrum is also shown. Interestingly, no calculated profile plotted in Fig. 5(a) could reproduce the high-energy hump at 7137 eV of the blue 3 spectrum. In order to reproduce this hump, distorted clusters with short Fe–O bonds (~0.19 nm), such as SB, were required (Fig. 5(c)). Because the low-energy (~7130 eV) components of such clusters are relatively low, $[FeCl(O)_5]$ profiles, such as 0.7M or 0.1M, were needed for the overall reproduction of the blue 3 spectrum. "FEFF-LC 2" is the best-fit result for blue 3. FEFF-LC 2 consists of 0.60 of 0.7M and 0.40 of SB, and gives a fairly good reproduction of the blue 3 spectrum, particularly for the white line and high-energy hump. This suggests that at least two types of Fe species co-exist at the blue 3 position: (i) the Fe species of which the local structure is similar to that of aquoiron(III) ions in dilute (<0.7 M) $FeCl_3$ solutions, $[Fe(Cl)O_5]$ (major); and (ii) the Fe species, including $[Fe(Cl)_2O_4]$, with shorter Fe–O bonds (minor). Thus, it can be concluded that the additional substitution of Cl (from an average of 1.4 to 2) and the increase in Fe–O bond length was related to the color change from blue to brown. Of note is the fact that the former point is consistent with the concentration dependence of the Fe^{3+} solutes in $FeCl_3$ aqueous solution.[30] The details of the short-bond species suggested for blue 3 (and other blue/white positions) are currently not clear, but one possible species is aquoiron(III) ions chemically adsorbed to SiO_2 in the water-glass gels, because the Si–O bond lengths (~0.16 nm) are shorter than Fe–O (~0.20 nm).

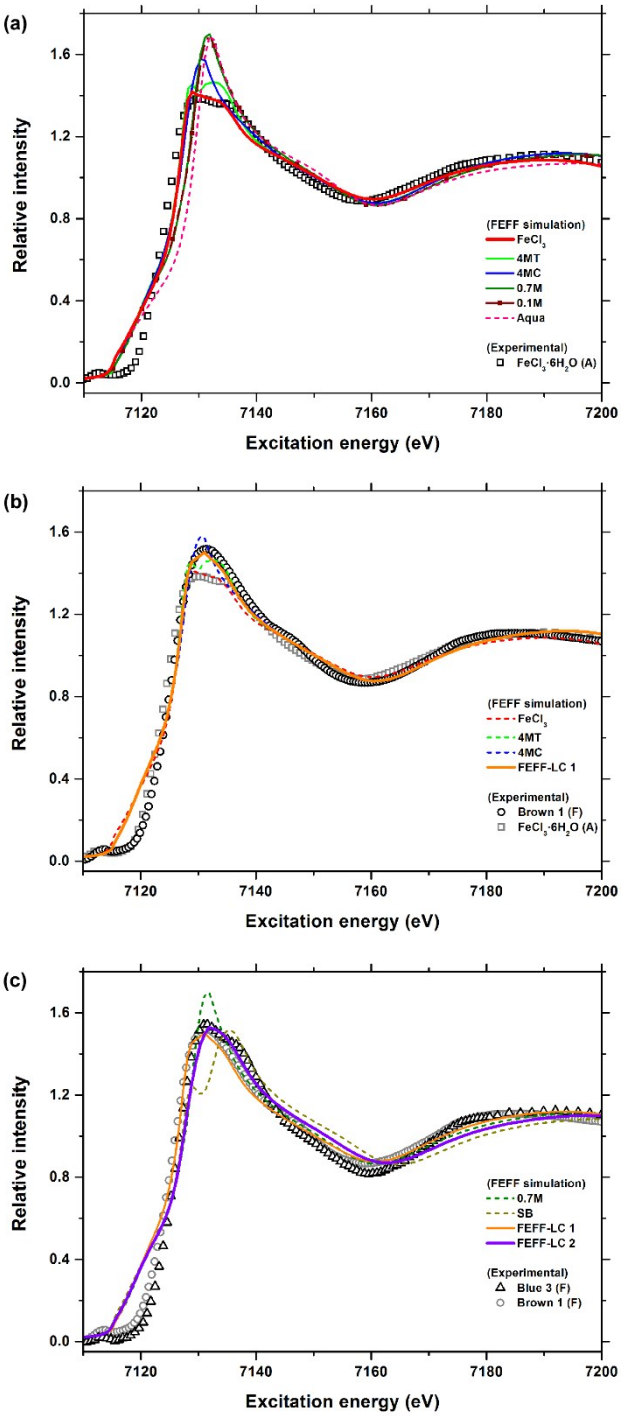

Fig. 5 Fe *K*-edge XANES profiles obtained by FEFF 8.02 calculations for the distorted octahedral clusters shown in Table 2. The profiles were compared with (a) the $FeCl_3 \cdot 6H_2O$ spectrum, (b) the brown 1 spectrum, and (c) the blue 3 spectrum. For comparison, the $FeCl_3 \cdot 6H_2O$ spectrum and the linear combination of the calculated profiles, "FEFF-LC 1" are also shown in Fig. 5(b). Similarly, the brown 1 spectrum and the linear combinations of the calculated profiles, "FEFF-LC 1" and "FEFF-LC 2", are shown in Fig. 5(c).

Conclusion

Summarizing the experimental results, we can derive the following conclusions for the multicolored pattern formation in the Fe system studied. Firstly, the Cl^- ions can be seen to play a key role in the formation of the brown bands, as demonstrated by the comparison of several control tubes. Secondly, through time-resolved XRF and position-dependent XANES, the properties of the brown bands and the contributions of Cl^- ions were clarified: (1) the brown bands formed due to the presence of concentrated Fe species in the water-glass gel, (2) the factors driving the accumulation of the Fe species were rather stable, and (3) the most likely local structure of the Fe species in the brown bands was $[Fe(Cl)_2O_4]$. Thirdly, the blue bands in tube A were independent of both the Fe concentrations in the gels and the local structure of the dominant Fe species (aquoiron(III)-related compounds, not PB). These independences could be due to the very small solubility product constants of PB species, which allow PB/PB-like compounds to form even under very low concentrations of both Fe^{2+} and $[Fe(CN)_6]^{3+}$. As a result, the brown bands were obscured by the blue colored PB-like compounds when high concentrations of Fe^{2+}, $[Fe(CN)_6]^{3+}$, and/or $[Fe(CN)_6]^{4+}$ were present, but became visible to reveal the multicolored patterns under very low concentrations of these ions.

Furthermore, the present study also demonstrated the presence of hidden RD processes in continuous, broad colored bands, including changes in metal concentration distributions and changes in the dominant chemical species. Although such processes have not been of great concern in traditional studies of precipitate patterns, these eccentric RD processes could be a subject of future research. The combination of time-resolved XRF and position-dependent XANES (possibly also time-resolved, position-dependent XANES and advanced, high-resolution XANES) will be helpful to explore not only intricate multicolored pattern formations, but also such "invisible" RD processes in continuous patterns.

The impressive patterns observed in the presently studied Fe system are not only worthy of considerable scientific attention by themselves, but can also potentially be applied to certain technological and/or analytical processes. For such applications, the basic aspects of the present system should be explored further. In particular, a greater understanding of the blue bands, including their detailed local structures, is a prerequisite. Furthermore, for comparison, extension to RD systems that form PB-analogues containing 3d-block elements other than Fe[23,39] would also be interesting. Such experiments are currently in progress.

Acknowledgments

The authors are grateful to Ms. M. Tatsuno, Ms. M. Mayusumi, and Ms. A. Kato of Japan Women's University for their help in sample preparation and data treatments. The XANES experiments at KEK-PF were conducted under proposal No. 2014G505. This study was supported by JSPS KAKENHI Grant Number 26410163 and Number 24710102.

References

1. H. Henisch, *Crystals in Gels and Liesegang Rings*, Cambridge University Press, Cambridge, 1988.
2. B. A. Grzybowski, *Chemistry in Motion: Reaction–Diffusion Systems for Micro- and Nanotechnology*, John Wiley & Sons, Chichester, 2009.
3. I. Lagzi, *Precipitation Patterns in Reaction–Diffusion Systems*, ed. I. Lagzi, Research Signpost, Kerala, India, 2010.
4. R. E. Liesegang, *Naturwiss. Wochenschr.*, 1896, **11**, 353.
5. B. A. Grzybowski, K. J. M. Bishop, C. J. Campbell, M. Fialkowski and S. K. Smoukov, *Soft Matter*, 2005, **1**, 114.
6. B. A. Grzybowski and C. J. Campbell, *Mater. Today*, 2007, **10**, 38.
7. T. Karam, H. El-Rassy and R. Sultan, *J. Phys. Chem. A*, 2011, **115**, 2994.
8. I. Lagzi, *Langmuir*, 2012, **28**, 3350.
9. M. Al-Ghoul, M. Ammar and R. O. Al-Kaysi, *J. Phys. Chem. A*, 2012, **116**, 4427.
10. L. Mandalian, M. Fahs, M. Al-Ghoul and R. Sultan, *J. Phys. Chem. B*, 2004, **108**, 1507.
11. Z. Shreif, L. Mandalian, A. Abi-Haydar and R. Sultan, *Phys. Chem. Chem. Phys.*, 2004, **6**, 3461.
12. S. Horvát and P. Hantz, *J. Chem. Phys.*, 2005, **123**, 034707.
13. M. Msharrafieh, M. Al-Ghoul, H. Batlouni and R. Sultan, *J. Phys. Chem. A*, 2007, **111**, 6967.
14. M. Al-Ghoul, T. Ghaddar and T. Moukalled, *J. Phys. Chem. B*, 2009, **113**, 11594.
15. I. Lagzi, B. Kowalczyk and B. A. Grzybowski, *J. Am. Chem. Soc.*, 2010, **132**, 58.
16. H. Nabika, M. Sato and K. Unoura, *Langmuir*, 2014, **30**, 5047.
17. M. West, A. T. Ellis, P. J. Potts, C. Streli, C. Vanhoof and P. Wobrauschek, *J. Anal. At. Spectrom.*, 2015, **30**, 1839.
18. L. Mino, G. Agostini, E. Borfecchia, D. Gianolio, A. Piovano, E. Gallo and C. Lamberti, *J. Phys. D: Appl. Phys.*, 2013, **46**, 423001.
19. H. Hayashi, *X-Ray Spectrom.*, 2014, **43**, 292.
20. BL-9C of KEK-PF: an in-situ XAFS beamline. http://pfwww.kek.jp/users_info/station_spec/xafsbl/9c/bl9c_e.html. (accessed August 2015).
21. A. L. Ankudinov, B. Ravel, J. J. Rehr and S. D. Conradson, *Phys. Rev. B*, 1998, **58**, 7565.
22. A. L. Ankudinov, C. E. Bouldin, J. J. Rehr, J. Sims, H. Hung, *Phys. Rev. B*, 2002, **65**, 104107.
23. A. A. Karyakin, *Electroanalysis*, 2001, **13**, 813.
24. S. C. Müller, S. Kai and J. Ross, *J. Phys. Chem.*, 1982, **86**, 4078.
25. S. Kai, S. C. Müller and J. Ross, *J. Phys. Chem.*, 1983, **87**, 806.
26. W. Seka and H. P. Hanson, *J. Chem. Phys.*, 1969, **50**, 344.
27. T. E. Westre, P. Kennepohl, J. G. DeWitt, B. Hedman, K. O. Hodgson and E. I. Solomon, *J. Am. Chem. Soc.*, 1997, **119**, 6297.
28. M. Wilke, F. Farges, P.-E. Petit, G. E. Brown Jr and F. Martin, *Am. Min.*, 2001, **86**, 714.
29. A. Bianconi, M. Dell' Ariccia, P. J. Durham and J. B. Pendry, *Phys. Rev. B*, 1982, **26**, 6502.
30. K. Asakura, M. Nomura and H. Kuroda, *Bull. Chem. Soc. Jpn.*, 1985, **58**, 1543.
31. P. Glatzel, L. Jacquamet, U. Bergmann, F. M. F. de Groot and S. P. Cramer, *Inorg. Chem.*, 2002, **41**, 3121.
32. L. Wang, T. Hu, J. Wu, Z. Xu, X. Zhang, D. Xu and G. Xu, *Mikrochimica Acta Suppl.*, 1997, **14**, 345.
33. F. de Groot, G. Vankó and P. Glatzel, *J. Phys.: Condens. Matter*, 2009, **21**, 104207.
34. J.-P. Rueff, L. Journel, P.-E. Petit and F. Farges, *Phys. Rev. B*, 2004, **69**, 235107.

35. H. Hayashi, *Chemical Effects in Hard X-ray Photon-In Photon-Out Spectra*, in *Encyclopedia of Analytical Chemistry*, ed. R. A. Meyers, John Wiley & Sonns, Chichester, 2014. DOI: 10.1002/9780470027318.a9389.
36. P. Glatzel and U. Bergmann, *Coord. Chem. Rev.*, 2005, **249**, 65.
37. H. Hayashi, *Anal. Sci.*, 2008, **24**, 15.
38. W. Błachucki, J. Szlachetko, J. Hoszowska, J.-Cl. Dousse, Y. Kayser, M. Nachtegaal and J. Sá, *Phys. Rev. Lett.*, 2014, **112**, 173003.
39. G. Fornasieri, M. Aouadi, E. Delahaye, P. Beaunier, D. Durand, E. Rivière, P.-A. Albouy, F. Brisset and A. Bleuzen, *Materials*, 2012, **5**, 385.